On the Simulation of a Heavy Vehicle Wake in OpenFOAM with Real-World Data

Keith A. Weinman[1(✉)], Henning Wilhelmi[1,2], James R. Bell[1], Daniela Heine[1], and Claus Wagner[1,2]

[1] DLR Göttingen, Institute of Aerodynamics and Flow Technology, Bunsenstr.10, 37073 Göttingen, Germany
keith.weinman@dlr.de

[2] Institute of Thermodynamics and Fluid Mechanics, Technical University of Ilmenau, Helmholtzring 1, 98693 Ilmenau, Germany

Abstract. Two computational approaches are taken to characterize the drag of a car driven behind a heavy vehicle under real conditions. The on-road approach uses velocity measurements, obtained from an array of static five-hole probes, to construct on-flow boundary conditions replicating the atmospheric dynamics encountered during an on-road measurement. The wind tunnel approach uses an oscillating flap system to control flow time and length scales upstream of a wind tunnel model. The amplitude and frequency of the flap motion is calibrated to reproduce length and time scales at on-road conditions under respective Reynolds and Strouhal number scaling. These approaches are evaluated against experimental measurements using Computational Fluid Dynamics (CFD) and demonstrates that they reproduce the aerodynamic drag and a significant part of the measured onflow condition for the car.

Keywords: DDES · Boundary reconstruction · Heavy vehicle wake · Real-world data · On-road tests · Oscillating flaps · RANS · Radial basis function · Vehicle drag prediction · Wind tunnel tests

1 Introduction

The paper is concerned with the prediction of drag, under real world conditions, of a compact car (length: 4.2 m, height: 1.4 m, width: 2m) following a medium box truck (length: 8 m, height: 3 m, width: 2.24 m) at a fixed distance of 50 m and at a constant speed of 27.776 m/s [1,2]. The configuration conforms to the definition of a two-vehicle platoon. The energy-saving potential of platoon configurations is discussed in several publications. For example, [3] demonstrates that numerical methods provide industrially relevant drag estimates for platoon configurations under both wind tunnel and real world conditions. The paper investigates how well CFD assesses real world unsteady flow effects on drag prediction for a two vehicle platoon configuration. An important difference between the on-road approach discussed in this paper and other published work is that the

© The Author(s), under exclusive license to Springer Nature Switzerland AG 2021
A. Dillmann et al. (Eds.): STAB/DGLR Symposium 2020, NNFM 151, pp. 504–513, 2021.
https://doi.org/10.1007/978-3-030-79561-0_48

influence of the leading vehicle on the trailing vehicle is modeled using an inflow boundary condition. By comparison the wind-tunnel approach generates onflow conditions characteristic of the on-road conditions for a wind tunnel model by directly perturbing the internal flow upstream of the model.

2 Methodology

In the on-road approach velocity measurements are sampled 250 Hz using a 2D array of eleven five-hole probes (located 1 m in front of the car). Lateral distances between the probe elements vary from 0.49 m to 0.98 m. Nine probes are located at a vertical height z = 0.5 m above ground with a further two being located along the array's symmetry axis at z = 1.1 m and z = 1.7 m. Velocity and pressure measurements are taken in the wake of the truck (data set W) and also with only the test vehicle on the road (data set A). Section 2.1 describes the construction of an inflow boundary condition, emmulating real test conditions using the data sets A and W. This boundary condition is used for Delayed Detached Eddy Simulations (DDES) within the framework of OpenFOAM [4]. For the wind tunnel approach experiments, using a 1:4 scale wind tunnel model, are conducted in the cross-wind facility Seitenwindkanal Göttingen (SWG) [5]. Oscillating flaps are used to perturb the oncoming flow. Flap frequency and amplitude are chosen to recreate scaled turbulent length and time scales deduced from on-road measurements. A 1:4 scaled version of the on-road measurement array is located 0.25 m in front of the wind tunnel model. Further details are found in [6] and [2].

2.1 Simulation of the On-Road Incoming Flow

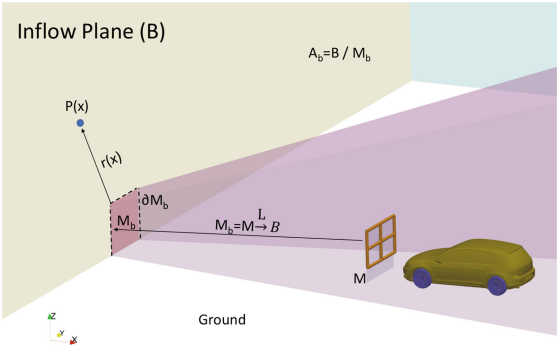

Fig. 1. The velocity field on M is reconstructed from probe measurements and is then mapped linearly (L) to the projection of M on the inflow plane B, M_b. The velocity on M_b is representative of the wake or the unsteady atmospheric boundary layer (ABL). Velocities of any point $P(x)$ on A_b, the relative complement of B on M_b, are computed by summing the atmospheric boundary layer velocity estimates at $P(x)$ with a weighted value ($W_f(x)$) of the velocity at the nearest point on ∂M_b (boundary of M_b). The weighting function $W_f(x)$ is a function of $r(x)$, the distance between $P(x)$ and the nearest point on ∂M_b.

The W and A data set correspond to several minutes of velocity measurements at a constant interval of 0.004 s between data points for each probe (both sets of data are assumed to start at t = 0). Figure 1 illustrates the car, the probe array, and a plane M extending from the ground to the top of the probe array with a width slightly larger than that of the probe array. The truck can be imagined to be positioned directly to the left of the inflow plane. The inflow boundary B is divided into two parts. The first part M_b, given by the projection of M onto B, is representative of either the resolved wake or the resolved ABL. The second part A_b, given by the relative complement of M_b on B such that $x \subset B \| x \not\subset M_b$, is representative of the ABL averaged across the span of the inflow plane. A no-slip boundary condition is defined on the edge on M lying along the ground with zero-gradient boundary conditions being defined on the remaining sides of M. A radial basis function method [7] is used to reconstruct the velocity field on M from either of the measured datasets A or W at each time step. The reconstructed velocity field on M is linearly translated (L) onto M_b. Two interpolation meshes are created on M and on B: the interpolation mesh on B is used by OpenFOAM tools to create the computational inflow boundary data at each time step. Spacing between nodes on the interpolation meshes is determined by the RBF shape parameter. A least-squares fit for a neutral ABL profile at each time step is generated with the W data sets using the friction velocity $u^s(t)$ as the design variable. Other log layer parameters are estimated from the literature. The velocity fields on the wake inflow M_b can be considered as resolved spatially filtered turbulent velocity data (the filtering is due to the influence of the reconstruction and measurement processes) while the velocities on A_b are time-varying mean velocities. The ABL velocity estimates are not conservative but provide a crude estimate of the spanwise averaged ABL conditions when the road tests were undertaken. Inflow turbulence on A_b is modeled directly via the turbulence model. Inflow turbulence intensities can be rescaled independently for both M_b and A_b. The weighting function $W_f(x)$ returns unity on the interior and boundary of M_b but decays to 0 as distance from the boundary of M_b increases outside of the wake. For this work $W_f(x)$ is defined as

$$W_f(x) = 1 - A \tanh(Br(x)), \tag{1}$$

where A and B are scalar coefficients of O(1). Weighting removes potential numerical difficulties and mimics the upstream diffusion of velocity between the wake and ABL. Turbulence intensities can be modified on M_b by rescaling the velocity fields The velocity field, now fully defined on B, is written as an OpenFOAM input file and stored on disk for each time step. Internal OpenFOAM tools linearly interpolate these files (in space and time) onto the computational mesh boundary during the solution process.

2.2 Simulation of Incoming Flow for the Wind Tunnel Model

Figure 2a illustrates the 1:4 scale model of the test vehicle inside the SWG facility. The CFD geometry includes a moving belt to simulate relative ground motion as well as tire rotation. The geometry of the flapped system is shown in Fig. 2b. The flap motion parameters are set with an oscillation frequency 10 Hz and an oscillation amplitude of 10 degrees. Sliding mesh algorithms are used to simulate flap motion. A 2D measurement rake at 1:4 scale is placed in the same relative position to the model as for the on-road measurements.

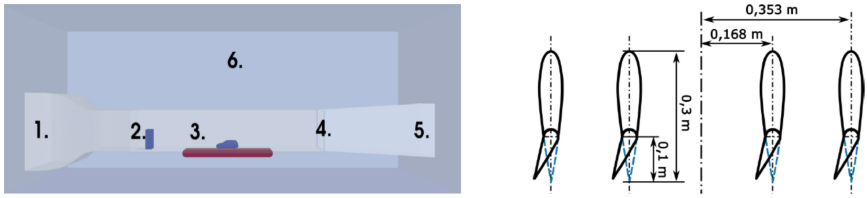

(a) View of SWG facility (b) Oscillating flap arrangement.

Fig. 2. Model mounted in SWT. SWT components: 1. Wind tunnel nozzle inflow, 2. oscillating flap system, 3. moving band, 4. pressure equalization gap, 5. WT diffuser outlet, 6. Plenum

2.3 Computational Set-Up

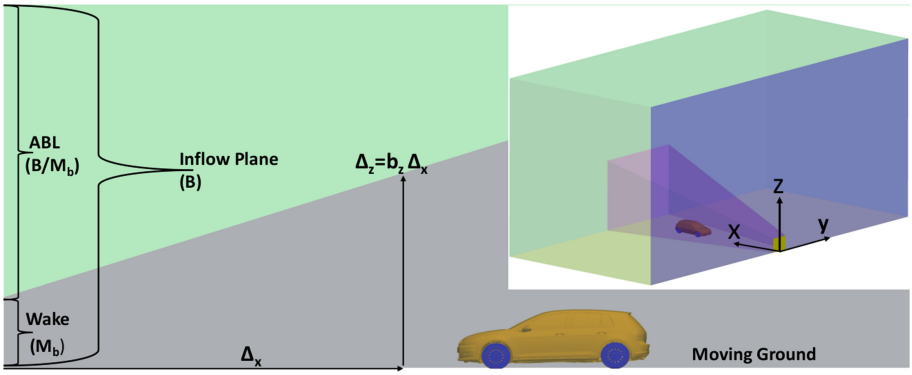

Fig. 3. The left figure illustrates the computational domain in the x-z plane. It shows the definition of the refinement region growth rate parameter b_z and the location of the wake portion of the inflow boundary plane M_b. The right figure illustrates the car within the computational domain. The purple region is a refinement zone to minimize the numerical dissipation influence on the wake velocity convected in from the boundary. Dimensions of the computational domain are given by $\Delta_x = 100\,\text{m}$, $\Delta_y = 100\,\text{m}$, $\Delta_z = 40\,\text{m}$. The car mid-axle position is located at x = 0 m and y = 0 m. Standard OpenFOAM inflow and moving ground boundary conditions are used, together with a farfield boundary at the outflow and other computational domain faces.

Figure 3 illustrates the computational domain. The interface between the wake region and the ABL is treated as a planar mixing layer as flow travels downstream, and the width of the wake region ($b_y = \Delta y_w/\Delta x_w, b_z = \Delta z_w/\Delta x$) grown in the downstream direction according to published measurements of mixing-layer growth. This interface bounds the refinement zone (set during mesh generation) where cell volumes are refined to reduce the on-flow numerical dissipation losses. The distance between the car and the onflow boundary can be varied only by generation of a new mesh. Distances of 50 m and 30 m are examined in this work. The current work uses the Engys OpenFOAM release 2.3.1 [8]. Baseline turbulence models are the Menter k-ω SST [9] and Spalart-Allmaras [10] turbulence models. The Delayed Detached Eddy versions of these models are used for the hybrid RANS-LES calculations. The filter width is chosen as 2Δ, where Δ is the cube root of the cell volume. A segregated pressure-based incompressible solver (pisoFoam) was used for all unsteady calculations. Steady calculations were performed using the simplecFoam solver. For all calculations an initial velocity field is generated using a potential flow method (potentialFoam). Time steps are chosen so that the Courant number is less than one for all control volumes. Second-order central differences are used for viscous fluxes, while a hybrid central-upwind scheme is used for inviscid fluxes. Best results were obtained using the local Courant number as the switching parameter between inviscid schemes. The linear system is solved using an Algebraic Multigrid method for the pressure correction equation, and with a stabilized Krylov Subspace method for the velocity and turbulence variables.

The CAD model used for the on-road calculations is taken from real geometry data provided by the manufacturers and is rescaled for the wind tunnel work. For this work OpenFOAM meshing tools return satisfactory high Reynolds number meshes. The meshing guidelines used follow previous work [11]. Surface length scales of 2 mm are used for the car and tires. The surface discretization length scale varies from 2 mm near the vehicle to the base length scale of 50 cm near the freestream boundaries. Eight levels of refinement are used in the wall normal direction of all no-slip surfaces. Writing L^n as the mesh length scale at a refinement level n, then $L^{n+1} = L^n/2$. Mean $y+$ values are in the ranges of 20–40 wall units. On the basis of several mesh refinement studies the final meshes used in this work are 180 million points for the on-road calculation and 64 million points for the wind tunnel calculation. A refinement level of 4 is used for the resolved wake region. Refinement is limited by available computational resources. For the on-road calculations the CFL number is limited to O(1), leading to times steps of the order 10^{-7} s. Identical CFD practices are used for the wind tunnel calculations.

Drag is not measured during the on-road tests and the wind tunnel measurements performed by FKFS in Stuttgart [6] provide validation data for drag estimation. The DDES variants of the base turbulence models return estimates of drag with differences of less than 3 drag counts against the experiment whereby one drag count is defined as 0.001 Cd. The averaged onflow velocity is used in the

normalization of surface pressure forces. Studies showed that Reynolds-averaged Navier Stokes (RANS) simulations returned errors of over 30 drag counts due to inadequate prediction of boundary layer separation (and reattachment) and vortex breakup effects. On this basis the DDES approach was adopted for turbulence modeling despite a significant increase in computational costs (see Sect. 5). Boundary layer resolving meshes require further computational overhead and were found to be very difficult to create with the standard OpenFOAM meshing library. Therefore wall functions are used to model near-wall turbulent stresses. Note that moving ground and tire rotation effects are modeled using standard OpenFOAM source term treatments.

3 Assessment of Incoming Velocity Fields

A qualitative assessment of the incoming flow generated by the on-road approach, comparing instantaneous streamwise u velocity components in time, is shown in Fig. 4. The velocity is underestimated in comparison with the experiment. Finer scale structures seen in the measured data are not present in the DDES results: the velocity field reconstruction filters out any length scales at the order of the inter-probe distance and below, and numerical dissipation effects are cumulative during a fluid particle's lifetime within the computational domain. Figure 4 also illustrates the frequency at which the maximum spectral energy is found for the spanwise v-component of velocity. Experiment and CFD are qualitatively in agreement but the spectral energy magnitudes are underpredicted at all probe positions with a significant one decade difference at z = 1.1 m. This height corresponds to a position where wake/ABL interface effects are expected and suggests that either additional time is required for higher-order velocity statistics to develop and/or that the computational modeling in this region is not fully adequate. Mesh resolution requirements need to be further increased in this region. Approximately 85% of the total control volumes are computed in DES mode but the DES length scales are too coarse for the proper development of the mixing layer interface.

In comparison to the differences observed in Fig. 4, the improvement in comparisons between the measured and computed onflow velocities for the wind tunnel approach is shown in Fig. 5. In this approach onflow components are precisely specified by single Fourier modes. The onflow boundary condition, given by the test section bulk velocity corrected for continuity at the nozzle inlet, is also well understood. The onflow velocity is dominated by the sinusoidal motion at the flap forcing frequency.

For both approaches the starting onflow disturbances are allowed to travel three car lengths past the vehicle before averaging is started. The averaging duration is more than 8 convective time units. Table 1 reflects that the on-road approach underpredicts the u component by up to 25%. This is due to the high-pass filter effect of the reconstruction process as well as the accumulation of low-order dissipation effects over the lifetime of the fluid in the computational domain. At a turbulence intensity of 6%, the mean u components for the reconstructed inflow boundary at $\Delta x = 30$ m (reconstructed from data collected at a

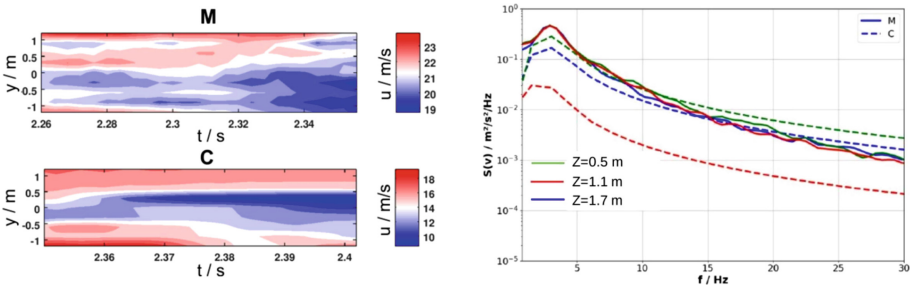

Fig. 4. The left figure shows a comparison of the measured (M) and computed (C) u-velocity component at z = 0.5 m above ground. The right figure shows a comparison of the computed and measured v-component power spectral densities for the three probes located on the array axis of symmetry.

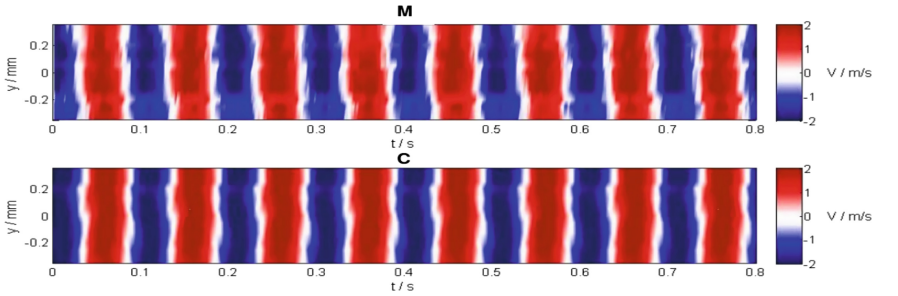

Fig. 5. Development of the v velocity component in the wind tunnel at z = 0.2 m above the test section floor. M: measured, C: CFD.

Table 1. Onflow statistics at the probe positions. M: Measured, B: CFD with block inflow profile. C: CFD with on-road approach. ∇ is the percentage difference against experiment.

	Mean						Standard deviation					
	M	B	C	C	C	C	M	B	C	C	C	C
On-road approach												
Tu_x %	6	6	2	6	6	10	6	6	2	6	6	10
Δx (m)	50	50	50	50	30	50	50	50	50	50	30	50
u (m/s)	24.5	22.1	18.7	18.8	19.3	18.1	2.8	0.46	1.05	1.53	0.9	1.73
v (m/s)	0.3	0.04	−1.9	−1.73	0.0	−2.7	1.8	0.23	0.50	1.77	0.5	1.37
w (m/s)	1.6	−0.4	−0.5	−0.5	0.77	0.5	1.0	0.27	0.28	1.13	0.8	0.61
Wind tunnel approach												
	M (m/s)		C (m/s)		∇%		M (m/s)		C (m/s)		∇%	
u	30.2		29.8		1.3		0.5		2.4		6.3	
v	0.0		−0.2		0.6		0.5		0.5		0.0	
w	0.0		0.2		0.6		0.3		0.4		0.3	

vehicle separation of 30 m) is comparable to that obtained for the reconstructed inflow boundary at $\Delta x = 50$ m. This is a significant observation and implies that if the onflow boundary is to be moved further downstream in order to reduce computational costs, then the inflow boundary velocity must be appropriately rescaled. However, if Δx is of the order of the wake core length, the flow impacting on the vehicle is highly correlated spatially and is not representative of on-road conditions at the vehicle separation distance. Differences between the velocity components v and w (magnified by the smaller magnitudes of these components) are due to slight differences in the atmospheric conditions. Removal of the mean signal from the measured data should be considered in future to avoid this uncertainty. Although the reconstruction method acts as a low-pass filter, the standard deviations of velocity for $\Delta x = 50$ m and a turbulence intensity of 6% agree qualitatively with the measured data. Most spectral energy is concentrated in the lower frequency modes (see Fig. 4) suggesting that further high-frequency filtering would be possible. The first and second statistical moments for the drag obtained with the wind tunnel approach agree more closely with measurements.

4 Assessment of Predicted Drag

Table 2. This table compares numerical estimates of the difference of the mean drag coefficient against drag at reference conditions. Standard deviations are given by δ. For both approaches the drag force has been normalized by the mean local onflow velocity. Tu_x is the inflow boundary turbulence intensity.

Δ_x (m)	Tu_x%	ΔC_d	δ_{C_d}
On-road approach: Reference [6] $C_d = 0.289$ at Δx = 50 m, $Tu_x = 6\%$			
50	2	29	0.13
50	6	0	0.13
30	6	6	0.03
50	10	−19	014
Wind-tunnel approach: Reference from experiment: $C_d = 0.291$			
–	6	8	0.02

Results obtained using the on-road approach in Table 2 suggests a functional dependence of aerodynamic drag on the inflow turbulence intensity. However, the data does not identify a trend. From the preliminary work noted in Sect. 2.3 the changes in drag between simulation techniques (RANS and DDES) are of the order of 20–30 drag counts, but were less than 10 counts for two different DDES models. Changes due to variations in the inflow turbulence intensity appear to be as significant as the change across simulation techniques, and this might support the notion that the onflow turbulence intensity is a parameter that should be stated when cross referencing vehicle drag estimations from different sources. The CFD and experimental determinations of drag differ by less than 10 drag

counts for the wind tunnel approach. There may be slight differences between the CFD and wind tunnel models which contribute to these differences. Another potential source of error is the prediction of the model blocking effect as well as the boundary layer growth on the wall of the tunnel. Care was taken to ensure that these are computed as accurately as possible, but slight differences may still accumulate and contribute to the 8 count difference observed. The standard deviation of the drag returned using the on-road approach is significantly higher for $\Delta x = 50\,\mathrm{m}$ in comparison to $\Delta x = 30\,\mathrm{m}$, however the variation in the mean drag is less than 10 counts. Correspondence between both CFD and experiment across both approaches for the mean drag is less than 10 drag counts.

5 Computational Resources

Resources of the Simulation Center of Aerodynamic Research in Transportation [12] are used for the work presented in the paper. Requirements for DDES simulations using reconstructed inflow boundary conditions scale at about 14 days for 1000 CPU's on a 120 million node mesh for one convective time unit. By comparison the RANS calculations, although significantly less precise, require approximately 48 h for convergence on 256 CPUs. DDES calculations performed for the wind tunnel require about 50% of the computational resources required for the reconstructed inflow simulations. This is due to the considerable smaller spatial resolution requirements.

6 Conclusions

The paper investigates the effect of changing on-flow conditions on the aerodynamic drag of a compact car which is driven behind a box truck under normal road conditions. Two CFD drag prediction approaches are assessed against both on-road and wind-tunnel experiments The on-road approach uses velocity measurements taken during on-road tests to reconstruct on-flow boundary conditions representative of those experienced during the on-road test. The wind-tunnel approach uses an oscillating flap system to control the on-flow turbulent length and time scales upstream of a wind tunnel model so that on-road conditions are approximately matched.

Both approaches create on-flow conditions which are consistent with real world observations. Both approaches return useful mean pressure estimations on the vehicle surface. Mean drag estimates are accurate to within 10 drag counts of the experimental data for both approaches using DDES. However significant resources are needed for both approaches when predicting second order statistical moments of the oncoming velocity and surface pressure. The wind tunnel approach uses well understood modeling and demonstrates the best agreement with measured oncoming flow dynamics, while the on-road studies suggests a dependence of mean drag on inflow turbulence levels that may be significant when comparing different drag data sets. Both of the approaches studied are complimentary and will be useful in investigations of unsteady vehicle aerodynamics.

However, some work remains in optimizing the on-road approach, particularly with regard to the computational cost of the technique and improving the energy content of the resolved flow.

Acknowledgement. The German Aerospace Center (DLR) would like to acknowledge the FAT Working Group 6 "Aerodynamics" for the realization of the Project and for excellent cooperation during the project period. The authors would also like to acknowledge Ms Annika Köhne for her assistance in the preparation of this paper.

References

1. Wilhelmi, et al.: Aerodynamic characterization of a compact car overtaking a heavy vehicle. In: New Results in Numerical and Experimental Fluid Mechanics XII. Notes on Numerical Fluid Mechanics and Multidisciplinary Design. Springer, Cham (2020). ISBN 978-3-030-25252-6, no. 794804
2. Wilhelmi, H., et al.: Simulation of transient on-road conditions in a closed test section wind tunnel using a wing system with active flaps. SAE Int. J. Passeng. Cars Mech. Syst. (0688), 1–13 (2020). https://doi.org/10.4271/2020-01-0688, ISSN 1946-3995
3. Davila, A., del Pozo, E., Aramburu, E., Freixas, A.: Environmental benefits of vehicle platooning. SAE Technical paper 2013–26-0142 (2013). https://doi.org/10.4271/2013-26-0142
4. Weller, H.G., Tabor, G., Jasak, H., Fureby, C.: A tensorial approach to computational continuum mechanics using object-oriented techniques. Comput. Phys. **12**(6), 620-631 (1998)
5. Haff, J., Richard, U., Kowalski, T., Loose, S., Wagner, C.: Wind tunnel experiments with a high-speed train model subject to cross-wind conditions. In: Pombo, J. (ed.) Proceedings on the First International Conference on Railway Technology: Research, Development and Maintenance, vol. 24. Civil-Comp Press, Stirlingshire (2012)
6. Wilhelmi, et al.: Aerodynamic characterization of a compact car driving behind a heavy vehicle. Notes on Numerical Fluid Mechanics and Multidisciplinary Design. Springer, STAB (2020)
7. Majdisova, Z., Skala, V.: Radial basis function approximations: comparison and applications. Appl. Math. Model. **51**, 728–743 (2017)
8. HELYX 3.2.1 - HELYX-Core User's Guide (2020)
9. Menter, F.R., Kuntz, M., Langtry, R.: Ten years of industrial experience with the SST turbulence model. Turbul. Heat Mass Transfer **4**(4), 625–632 (2003)
10. Spalart, P.R., Deck, S., Shur, M.L., Squires, K.D., et al.: A new version of detached-eddy simulation, resistant to ambiguous grid densities. Theoret. Comput. Fluid Dyn. 20(3), 181195 (2006). https://doi.org/10.1007/s00162-006-0015-0
11. Weinman, K.A., Fragner, M., Deiterding, R., Heine, D., et al.: Assessment of the mesh refinement influence on the computed flow-fields about a model train in comparison with wind tunnel measurements. J. Wind Eng. Ind. Aerodyn. **179**, 102117 (2018). https://doi.org/10.1016/j.jweia.2018.05.005
12. http://scart.dlr.de/site/index.pdp (2020)